

See discussions, stats, and author profiles for this publication at: <https://www.researchgate.net/publication/304779905>

# The effect of triple ion beam irradiation on cavity formation on pure EFDA iron

Article · July 2016

DOI: 10.1016/j.jnucmat.2016.06.043

---

READS

18

5 authors, including:



[Marcelo Roldán](#)

Centro Investigaciones Energéticas, Medio...

4 PUBLICATIONS 6 CITATIONS

SEE PROFILE



# The effect of triple ion beam irradiation on cavity formation on pure EFDA iron

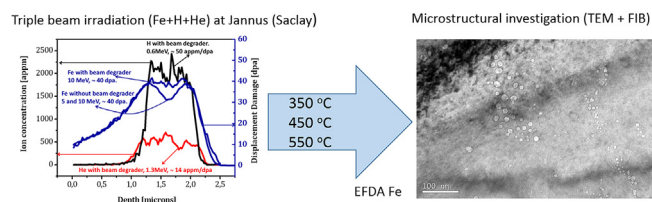


M. Roldán<sup>a,\*</sup>, P. Fernández<sup>a</sup>, R. Vila<sup>a</sup>, A. Gómez-Herrero<sup>b</sup>, F.J. Sánchez<sup>a</sup>

<sup>a</sup> National Fusion Laboratory-Fusion Materials, CIEMAT, 28040, Madrid, Spain

<sup>b</sup> National Centre of Electronic Microscopy, Complutense University, 28040, Madrid, Spain

## GRAPHICAL ABSTRACT



## ARTICLE INFO

### Article history:

Received 29 March 2016

Received in revised form

21 June 2016

Accepted 26 June 2016

Available online 2 July 2016

## ABSTRACT

Pure EFDA Iron was irradiated under triple ions beam (Fe + He + H) at 350 °C, 450 °C and 550 °C respectively to a nominal 40 dpa with a uniform He concentration of ~14 appm He/dpa and H content of ~50 appm H/dpa at depth between 1 and 2 μm.

Cavity characteristics (size, morphology, distribution and population) at each irradiation temperature have been thoroughly studied by TEM using FIB lamellae, showing bubble formation at all irradiation temperatures with several differences between one to another experimental condition. At 350 °C homogeneous distribution of small cavities with sizes in the range of 2–4 μm was observed. However, irradiations at 450 °C and 550 °C led to non-homogeneous distribution of cavities with a wide range of sizes. Additionally, it was detected at these temperatures, preferential nucleation of bubbles within the ferritic grains exhibiting rounded and faceted shapes. Faceted cavities with sizes larger than 16 nm were detected at 450 °C and 550 °C.

© 2016 Elsevier B.V. All rights reserved.

## 1. Introduction

Nowadays, one of the most important challenges in the development of fusion energy is to predict and mitigate the effects of large levels of transmuted gas atoms (He + H) along with high displacement damage produced by high energy neutrons that affects the mechanical properties of the structural materials and gives rise to phenomena like swelling [1]. In fact, radiation effects

produced by the interaction of He atoms with displaced atoms and H are still a key issue. The understanding of the macroscopic effects of cavity (bubbles, voids) formation due to He accumulation on the structural materials requires further research at different levels: experimental observations by TEM in basic and simple metals (model alloys) and modeling. A primary objective of such modeling and its associated experiments is to predict the dominant mechanisms that control the nucleation, diffusion and growth kinetics of bubbles and/or voids.

Different experimental approaches have been extensively used to study He effects for a wide variety of materials and conditions. The most notable irradiation techniques include multi-ion beam

\* Corresponding author. National Fusion Laboratory, CIEMAT, Avda. Complutense, 40, 28040, Madrid, Spain.

E-mail address: [marcelo.roldan@ciemat.es](mailto:marcelo.roldan@ciemat.es) (M. Roldán).

irradiation [2,3] neutron irradiation in mixed fast-thermal spectrum fission reactors carried out on alloys that contains naturally, or have been doped with, Ni and/or B [4–6], in situ He implantation in mixed spectrum fission reactors [7] and spallation proton-neutron irradiation [8–10]. All of these methods present limitations and none of them simulate fusion neutron spectra (14 MeV). However, all these irradiation tools closely integrated contribute to understand the key role of He on void swelling.

Triple ion beam irradiations are very useful to study the cavity nucleation mechanisms since the irradiation parameters can be well controlled and in many cases selectively and widely varied. This method, based on carefully designed experiments (temperature, radiation damage, He/dpa and H/dpa ratios), is a very attractive approach to identify and quantify key processes to calibrate advanced physical models.

Tanaka's [11] experiment has been used during a long time as a model to understand the synergetic effect of triple simultaneous irradiation in steels (radiation damage produced by Fe + H + He). However, some doubts appeared on repeated (but unpublished) experiments where these effects were not found. This led to the need for a replication of this experiment in Europe to confirm, deny or complete these results.

In the 70s, the scientific community had developed an extensive knowledge about nuclear fission and the effect of fission neutrons on structural materials. However, with regard to nuclear fusion, whose idea began to be developed slowly, it grew the need of emulating the neutron environment which would take place in the future nuclear fusion reactor, but avoiding the use of neutrons to facilitate microstructural and mechanical studies by means of charged particles (avoiding nuclear activation, very long irradiation experiments or, even, the difficulty to access to facilities that work with neutrons). This idea was materialized in a workshop that took place in Washington in 1976. Afterwards, a very interesting review paper was published which covered all side effects to consider when designing experiments using charged particles to simulate neutron radiation [12]. Especially relevant are the effects that are atypical of neutron environment such as non-isotropic particle flux, limited irradiation volume, surface effects and temperature and displacement rates gradient induced by the beam among others. It is, therefore, a great starting point to consider when it is requested to use charged particles to emulate neutrons, and more specifically to use of triple ion beam to obtain a clearer microstructural picture, which is the major goal of this research.

Lewis et al. [13] in 1979 published one of the first reported experiments using a new method with two Van de Graff accelerators to emulate nuclear fusion environment through the use of three ion beams: one accelerator produced  $\text{Ni}^{2+}$  to create a high atomic displacement density and the other one with a mixture of molecular He and deuterium which were injected so as to come to stop within the damaged region in order to simulate transmutation-produced He and H. Microstructure was studied thoroughly [14] and it was observed how hydrogen produced microstructural damage, even producing an unstable phase, however, the amount of H introduced into the specimen was really high which can lead an atypical embrittle mechanism.

Regarding material, iron is the base element of more complex alloys (such as ferritic-martensitic steels or oxide dispersed strengthened steels) candidate as structural materials for first wall and blanket applications, in which to know the effect of neutron irradiation is a critical point to be able to develop powerful damage modeling to predict the detrimental radiation effect on mechanical properties. The first step was achieved, which was the developing of a method to emulate neutron irradiation with ion beams, however, it was necessary to understand what occurs in the microstructure in terms of dislocation density, cavities and swelling, and

how these radiation products are related with irradiation parameters such as irradiation temperature, ion flux, dose rate, etc. to obtain reliable experimental data to validate these models. As mentioned, starting with iron [15,16] and comparing the observations with the ones carried out on neutron irradiated iron specimens [17].

In the late 1980 a triple beam facility was designed [18] and the first one, at least for this purpose, was built some years after in Japan [19]. Nowadays, it is possible to use some other facilities around the world, such as JANNuS in France or LLNL in USA. In those facilities are commonly used iron as displacement cascades producer (since Fe is the major element) and He along to H as transmutation gases. All of them are injected into the specimen with different energies, irradiation temperatures, ion fluxes etc. for the purpose of correlating microstructure with irradiation parameters, trying to recognize and minimize the side effects due to the nature of charged particles instead of neutrons.

It has been reported the synergistic effect of He atoms plus displacement cascades (irradiated with Al) [20] by means of dual beam irradiation, which seems to be very drastic at high temperatures in terms of swelling increase. Nowadays, the role of He has been demonstrated and it is better known than years ago, not only regarding microstructural evolution but also on mechanical properties [21,22]. Nevertheless, there are still some unknowns such as the role of H on microstructure with He and dpa. There are many evidences about the detrimental effect of H on mechanical properties of iron especially at temperatures around 550 K [23], however there is a lot to discover regarding the synergistic effect of He, H and dpa at different irradiation temperatures.

Taking into account all the aforementioned, it is clearly necessary (almost mandatory) to design new experiments using double and triple ion beam facilities trying to unmask all the irradiation induced effects and to gain insights about the major role of He, H and Fe on microstructural evolution in order to provide reliable data for modeling.

## 2. Experimental procedure

### 2.1. Materials

The material investigated in this work is pure Fe fabricated under contract EFDA-06-1901. Details of fabrication, analysis and microstructural characterization are given in Ref. [24]. This model alloy was delivered on recrystallized state after a cold reduction of 70% and heat treatment at 700 °C/1 h followed by air cooling with the chemical composition indicated in Table 1.

After the final heat treatment, the material presents a mean grain size of 183  $\mu\text{m}$  with minimum and maximum sizes of 4 and 650  $\mu\text{m}$ , respectively. The dislocation density, that was calculated by the method of mean intercept length taking 10 elementary surfaces of  $2 \times 2 \mu\text{m}$ , resulted being very low ( $\sim 1.2 \cdot 10^8 \text{ cm}^{-2}$ ) and its distribution was heterogeneous.

### 2.2. Triple ion beam ( $\text{Fe}^{3+}+\text{He}^++\text{H}^+$ ) irradiation

The triple simultaneous irradiation was carried out at the Joint Accelerator for Nanoscience and Nuclear simulation (JANNuS)

**Table 1**  
Chemical composition of the pure EFDA Fe.

Alloy	C ppm	S ppm	O ppm	N ppm	P ppm	Cr ppm
Fe	4	2	4	1	<5	<2

located at CEA Saclay (France) [25].

The simulation was carried out by using the full-cascade mode in SRIM. A displacement energy for Fe atoms of 40 eV [26] was used in order to calculate the total vacancies produced by the irradiation.

Originally, the irradiation was designed to use a beam degrader with three beams in order to simulate the fusion environment over the depth range from 1 to 2  $\mu\text{m}$ , using implantation energies of 10 MeV ( $\text{Fe}^{3+}$ ), 1.3 MeV ( $\text{He}^+$ ) and 600 KeV ( $\text{H}^+$ ) to produce damage of  $\sim 40$  dpa,  $\sim 500$  appm He and  $\sim 2000$  appm H. The dpa contribution arising from He and H implantation was negligible compared to that of the Fe ions whose damage rate at the peak was around  $1.7 \times 10^{-3}$  dpa/s for all the irradiations. This irradiation configuration leads to He/dpa and H/dpa ratios of  $\sim 12.5$  and  $\sim 50$ , respectively. Unfortunately, during irradiation at 550  $^{\circ}\text{C}$ , some Al foils of the Fe beam degrader were destroyed due to the Fe beam flux and it was decided to perform the  $\text{Fe}^{3+}$  irradiation without beam degrader in the other temperatures (350  $^{\circ}\text{C}$  and 450  $^{\circ}\text{C}$ ), using instead two individual energies of 5 and 10 MeV with a flux ratio of 1:3. With this new implantation configuration the damage level and the He/dpa and H/dpa ratios were practically the required ones; 40 dpa,  $\sim 14$  He/dpa and  $\sim 50$  H/dpa (Fig. 1). The irradiation was carried out on 3 mm diameter disks of pure Fe.

### 2.3. Microstructural characterization

A Zeiss Focused Ion beam (FIB) microscope was used to micro-machine thin transparent lamellae, which included both damaged-implanted and undamaged regions. The extracted lamella was thinned in different paths (Fig. 2) in order to study the homogeneity of the nucleation defects. The microstructure of each path was studied separately in different lamellae and the implantation depth (2  $\mu\text{m}$ ) was divided into bins of 250 nm to do the calculations.

TEM observations were performed on a JEOL JEM 2100 and JEOL JEM 3000F operating at 200 and 300 kV respectively. Cavities were characterized by the through-focus bright field sequence method with the specimen tilted away from the Bragg condition, in order to avoid, as much as possible, the orientation contrast which makes impossible the observation of the cavities. The magnification was adjusted to provide optimal visibility for each irradiation temperature. All the detected cavities were measured using an image software (Leica LAS) and located with respect to the irradiation surface. The foil thickness of each lamella path was calculated by convergent beam electron diffraction (CBED) as shown in Fig. 2.

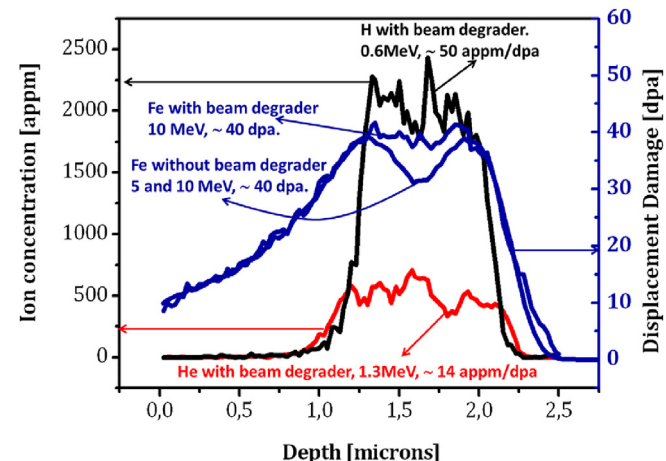


Fig. 1. SRIM calculation for triple ion irradiation at Jannus on pure EFDA Fe.

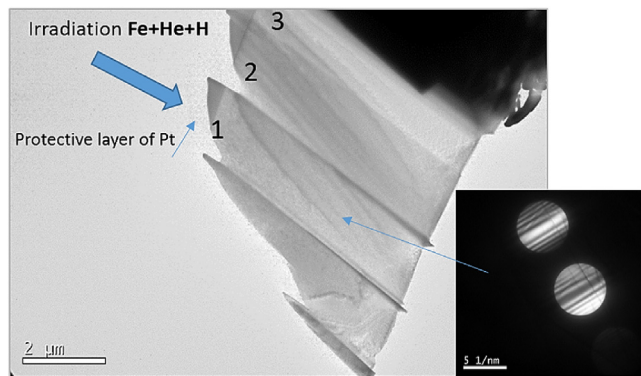


Fig. 2. Lamella of pure EFDA Fe showing 3 paths (numbered from 1 to 3) with their characteristic thickness measured by CBED (one of them is showed as example).

Finally, the number density and swelling per bin (in terms of volume fraction) were calculated.

With this methodology it was possible to obtain a sufficiently large TEM observable area and therefore, very good statistics.

It was not determined whether the cavities observed were filled or not with Helium. As the ratio He/V and cavities pressure remain unknown, it is not possible to distinguish if the defects were bubbles or voids, hence in this paper they were called simply “cavities”.

## 3. Results

### 3.1. As received condition

Due to the importance of the microstructure previous to the irradiation, it is necessary to perform a TEM analysis on some pure EFDA Fe samples in order to analyze the dislocation density and any other microstructural features which were able to interact with the irradiation defects.

The sample of pure EFDA Fe was cut and thinned up to less than 100  $\mu\text{m}$ , then the 3 mm disc were punched by using a disc punch. Finally, it was prepared by electropolishing with TENUPOL device using  $\text{H}_2\text{SO}_4$  (20%) and methanol (80%) at 15  $^{\circ}\text{C}$  and around 9 V.

The dislocation density was calculated using the mean interception length method with 5 lines per micrographs. For this calculation, 10 micrographs, located around the jet-polished hole and separated far enough from one another to not count the same dislocation network, were used. It is possible to see two of them in Fig. 3 a and b, taken in TEM bright field imaging condition and random crystal orientation.

The TEM observations are in good agreement with the manufacturer report [24] except for the dislocation density number. It was  $\rho = 1.44 \times 10^{10} \text{ cm}^{-2}$  in the “as-received” condition, just before the irradiation. This number is 2 orders of magnitude larger than the value given by the manufacturer.

### 3.2. Irradiation at 350 $^{\circ}\text{C}$

The different paths of the lamella extracted from the pure Fe specimen irradiated at 350  $^{\circ}\text{C}$  with triple ion beam were analyzed searching nucleated cavities from the very surface up to 2.25  $\mu\text{m}$  in depth. At this irradiation temperature, all the cavities showed a round morphology with random distribution within the matrix. Regarding cavity diameter, their size depends strongly on the lamella depth. Mainly, many cavities were detected very close to the irradiated surface up to the first 500 nm. Subsequently, the population starts decreasing until 1  $\mu\text{m}$  (Fig. 4). At a deeper position, cavities were observed, but they are very small.

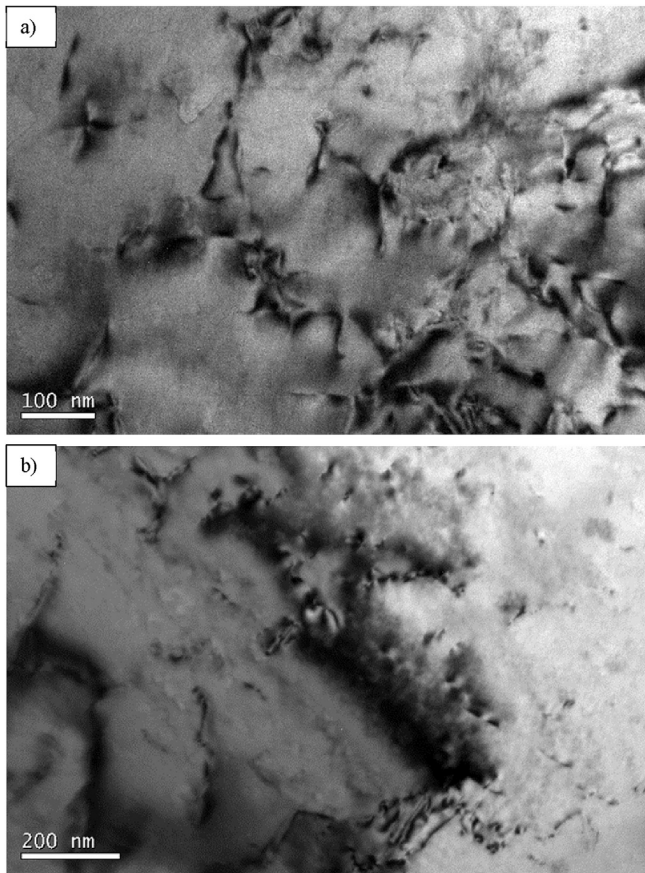


**Fig. 3.** TEM micrograph of pure EFDA Fe in as received condition showing some dislocations, at two different positions, a)90° and b)180° around the hole.

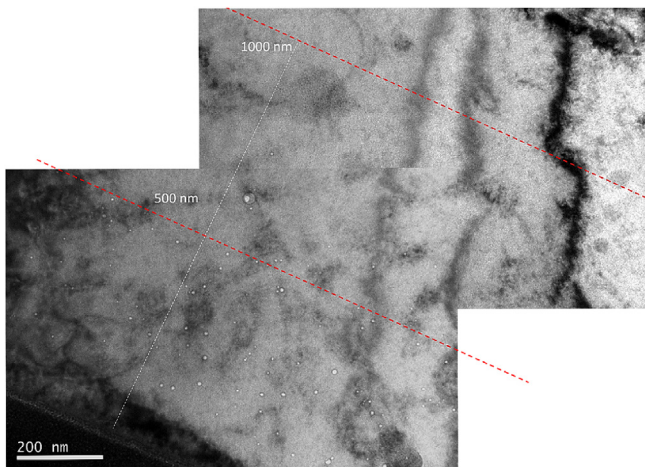


**Fig. 4.** Under-focus TEM images of pure EFDA Fe irradiated with triple ion beam up to 40 dpa, ~14 He/dpa and ~50 H/dpa at 350 °C. Cavity distribution from the surface up to 1 μm.

The cavity population suddenly increased at 1.5 μm as can be seen in Fig. 5. However, although the amount of cavities increased, the impact on swelling is very low since the maximum measured diameter of those cavities was less than 5 nm.

Pure Fe irradiated with triple ion beam at 350 °C showed cavities distributed within the matrix with a wide range of diameters from 1 nm up to 18 nm maximum. Analysis of images taken along

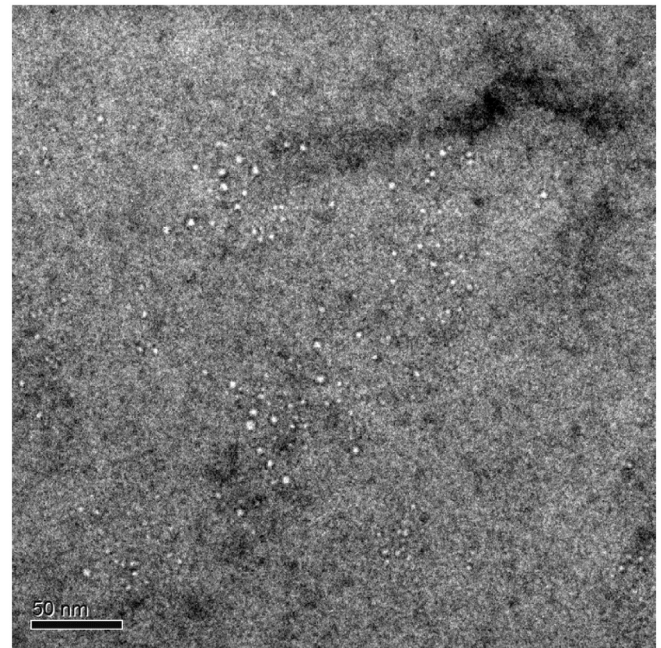


**Fig. 5.** Under-focus TEM micrograph of pure EFDA Fe irradiated with triple ion beam up to 40 dpa, ~14 He/dpa and ~50 H/dpa at 350 °C. Cavity distribution at 1.5 μm far from the surface.

the irradiated region showed that most of the largest cavities ( $\geq 4$  nm) are located between 0 and 500 nm, but they were also found at larger depths (Fig. 6 a). As it can be seen in the figure, beyond 750 nm the population density increases as the size decreases, reaching a nucleation maximum of  $\sim 3.5 \times 10^{22} \text{ m}^{-3}$  at 1500 nm, as seen in Fig. 5. Taking into account the SRIM calculation (Fig. 1), it would be expected that the largest cavities were located between 1 and 2 μm due to reported synergistic effects between He and H [11], together with the maximum dpa value. Although cavities with a wide range of sizes were detected and measured, from Fig. 6 a) it can be deduced that the largest population densities correspond to sizes lower than 2 nm and sizes between 4 and 6 nm. It is clear that the irradiation conditions performed in this work at 350 °C produced a bimodal range of cavity diameter. Fig. 6 b) shows the corresponding variation of volume fraction in function of implantation depth. Note that the swelling is very low since its value did not exceed 0.2%; indeed, the maximum value in population density has not much influence on swelling due to the size of the cavities.

The cavity density number indicates the cavity population per  $\text{m}^3$ . Fig. 6 c) shows a rising trend as the irradiation depth increases with a maximum between 1500 and 2000 nm according to the maximum damage area.

### 3.3. Irradiation at 450 °C

At this irradiation temperature, the cavities are non-uniformly distributed, exhibiting preferential formation with circular and polyhedral-faceted shape; unlike the cavities detected in the specimen irradiated at 350 °C, which are all circular. Fig. 7 shows the overview of the irradiation depth from the very surface up to depths larger than 2 μm. Most of the cavities, regardless of their size, nucleated following a determined order. By increasing the magnification, it is possible to observe with more detail different clusters of cavities that nucleated approximately at 1 μm further from the irradiated surface (Fig. 8 from the red rectangle in Fig. 7).

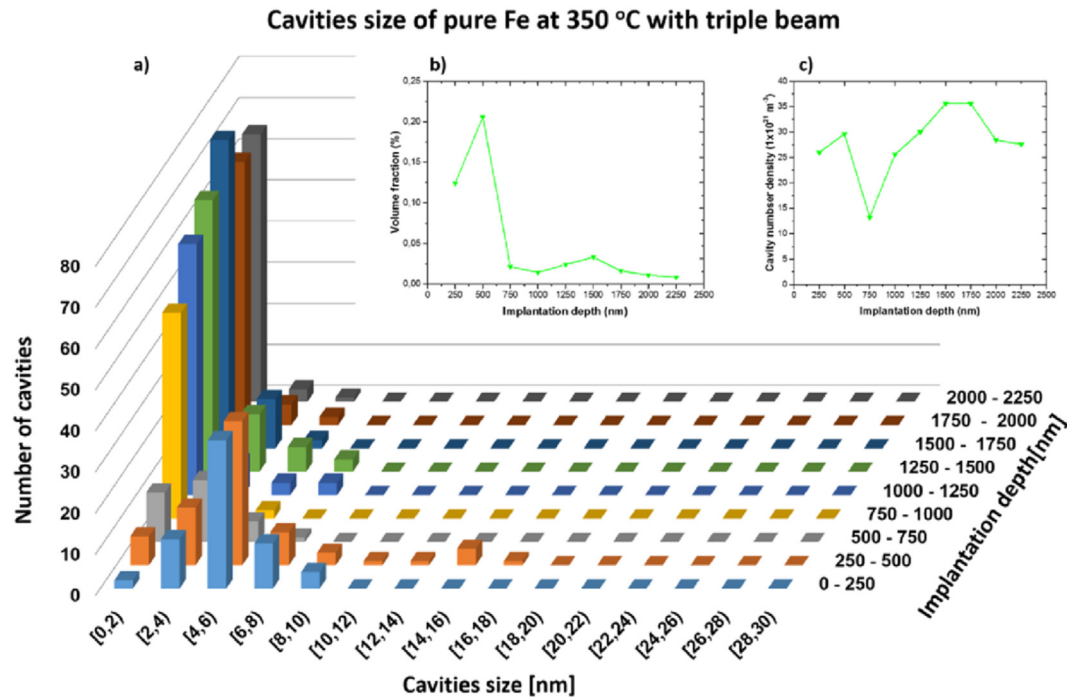


**Fig. 6.** a) Cavity size and b) Volume fraction in function of irradiation depth and c) cavity density number of pure EFDA Fe irradiated by triple ion beams to 40 dpa,  $\sim 14$  He/dpa and  $\sim 50$  H/dpa at 350 °C.

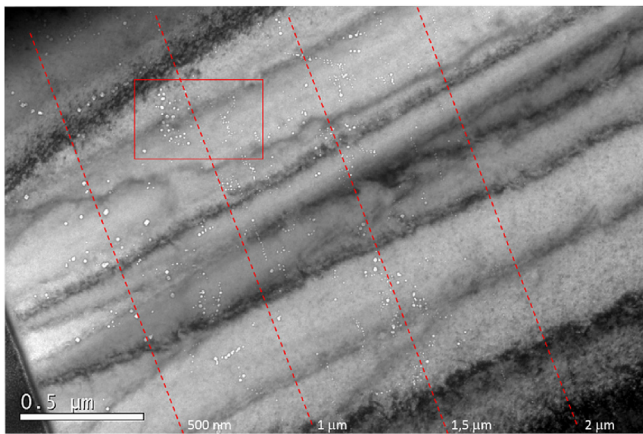


**Fig. 7.** Bright field TEM image showing the cavity distribution, size and morphology on pure EFDA Fe irradiated by triple ion beams to 40 dpa,  $\sim 14$  He/dpa and  $\sim 50$  H/dpa at 450 °C.

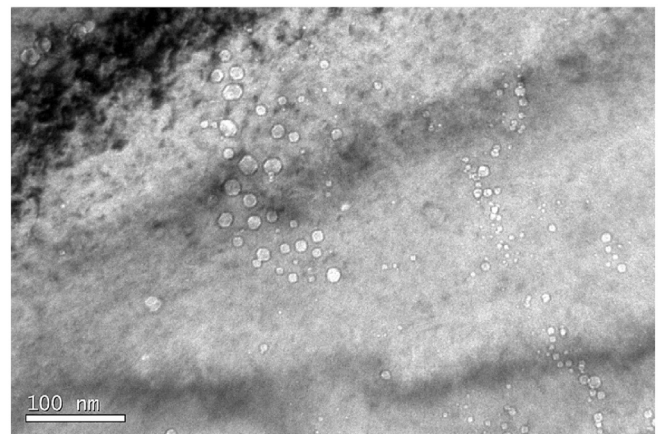


**Fig. 8.** Bright field TEM image showing different clusters of cavities on pure EFDA Fe irradiated by triple ion beams to 40 dpa,  $\sim 14$  He/dpa and  $\sim 50$  H/dpa at 450 °C.

The mentioned picture shows clearly how the clusters have two different average sizes, which means that the large cavities coexist with the ones with similar size and vice versa. This heterogeneous distribution is probably due to the interaction between local variations in the microstructure such as dislocations (which were detected on the as-received condition) or even the interaction between grain boundaries and the cavities, which can interfere on nucleation. Those microstructural characteristics may be invisible under the TEM operation conditions used in this work to identify them.

As a result of the analysis of the entire irradiated zone at 450 °C (Fig. 9), the cavities showed a wide range of sizes from 1 up to 18 nm. As the depth of implantation increases, a few cavities with sizes around 20 nm were also detected. The largest cavities ( $\geq 4$  nm) were observed within the damage region from 500 to 2000 nm. The

most common diameter range detected was the one between 2 and 4 nm (Fig. 9 b) shows the changes in volume fraction of the cavities in function of the implantation depth. As it can be seen, at 450 °C the swelling remains low, but in comparison with the irradiation at 350 °C, the irradiation temperature increment of 100 °C enhances the swelling up to approximately 1.2%. The cavity population, as well as their size, increases rapidly up to 750 nm, suggesting the bimodal bubble-void transition. But then, both parameters decrease gradually reaching another minimum out of the irradiation peak. This fact is observed in the density cavity number, Fig. 9 c).

### 3.4. Irradiation at 550 °C

The last pure Fe specimen analyzed was the one irradiated at

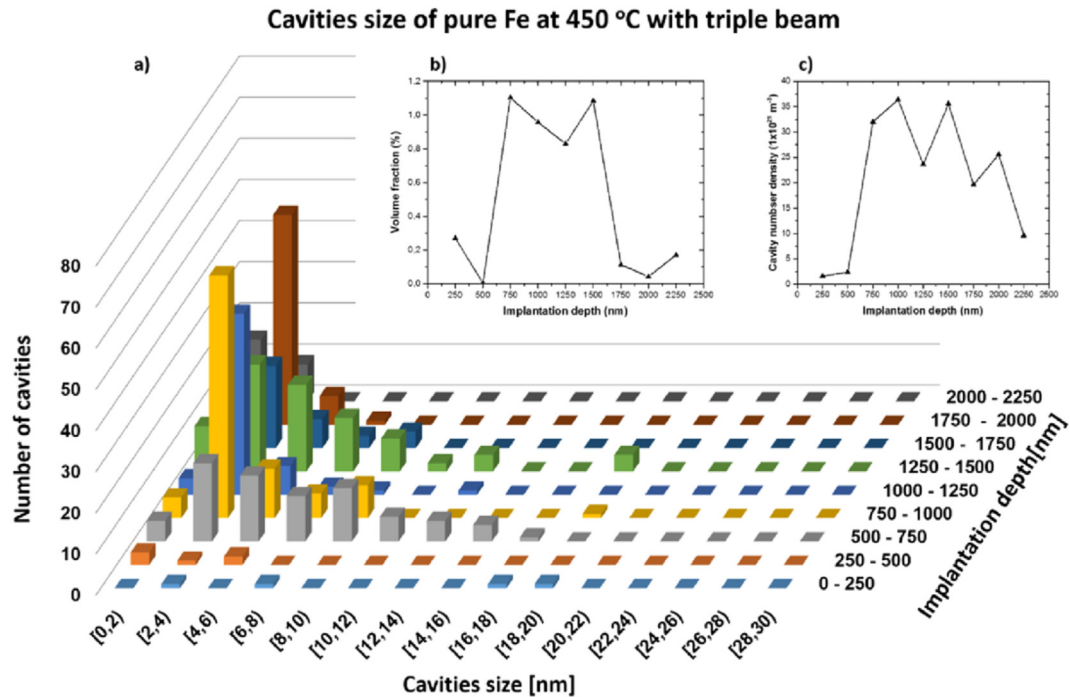


**Fig. 9.** a) Cavity size and b) Volume fraction in function of irradiation depth and c) cavity density number of pure EFDA Fe irradiated by triple ion beams to 40 dpa, ~14 He/dpa and ~50 H/dpa at 450 °C.

550 °C. Cavities from the implanted surface up to 2250 nm were observed, with different size and population density depending on their location on the damaged region. After an exhaustive analysis by TEM of each lamella path of this specimen, the observations indicated that the number of nucleated cavities between the surface and 500 nm are low as well as their size comparing this sample with the other irradiation conditions. The maximum size measured in this region was 4 nm. From that depth, the cavities experienced a growth in population and mainly, an increase in size due to swelling. An overview of one of the path is presented in Fig. 10, which characterizes all the irradiation damage area from the surface up to 2 μm and shows the aforementioned cavity characteristics. With regard to the shape, cavities detected presented both circular and polyhedral-faceted shape (Fig. 12), as in the case of irradiation at 450 °C.

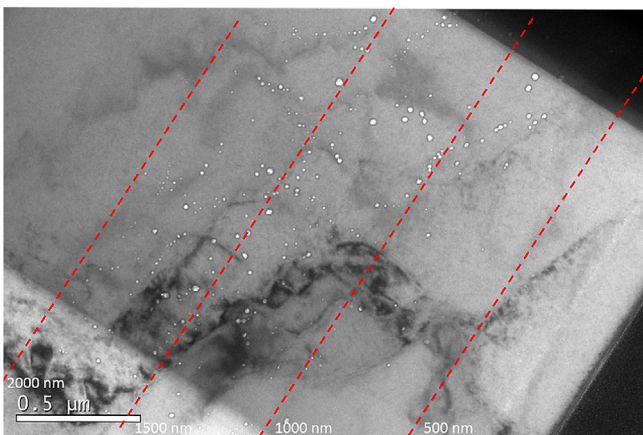


**Fig. 10.** Overview of the irradiation area from one lamella path extracted from the specimen irradiated with triple beam at 550 °C.

The population and cavity size in function of the implantation depth is shown in Fig. 11 a). From this figure, it is deducible that the maximum population of cavities exhibiting sizes  $\geq 4$  nm is mostly placed inside the damage peak, which is located between 1 and 2 μm depth. The highest irradiation temperature clearly leads to an increase of the cavity size. Large faceted cavities from 6 to 30 nm have been detected between 750 and 1500 nm. At this irradiation temperature, the maximum calculated volume fraction was 1.4%, obtained at 1250 nm (Fig. 11 b). Clearly, the effect of large cavities on swelling is critical compared with many small cavities. Although this value is the highest swelling rate of the three irradiation temperatures, it is still low when compared with other triple beam experiments [11]. Regarding the cavity density number, this value increases as the irradiation depth increases, achieving its maximum  $\sim 2.5 \times 10^{22} \text{ m}^{-3}$  at 1500 nm.

At 1250 nm, the maximum swelling value was obtained as well as the largest cavity size, ~30 nm. It corresponds with maximum He/dpa and H/dpa ratio and maximum dpa level. Fig. 12 shows in a more detailed way, some micrographs taken from the depth where it is possible to see the alignment of the cavities along dislocations or grain boundaries as well as the size distribution. The nucleation is completely preferential regardless of the cavity size.

#### 4. Discussion

As shown in Figs. 6, 9 and 11, the cavities, regardless of their diameter, have been detected outside of the damage peak (confined mostly between 1 and 2 μm, Fig. 1) for all the irradiation temperatures. Those observations would indicate that the nucleation does not depend strongly on irradiation temperature, but when cavity size is taken into account, the aforementioned parameter seems to be critical, as well as for the resultant peak swelling.

A well-known effect called *interstitial injection* is observed when Fe ions, used as displacement cascade producers, act as interstitials at their stopping range. This strongly decreases void nucleation and

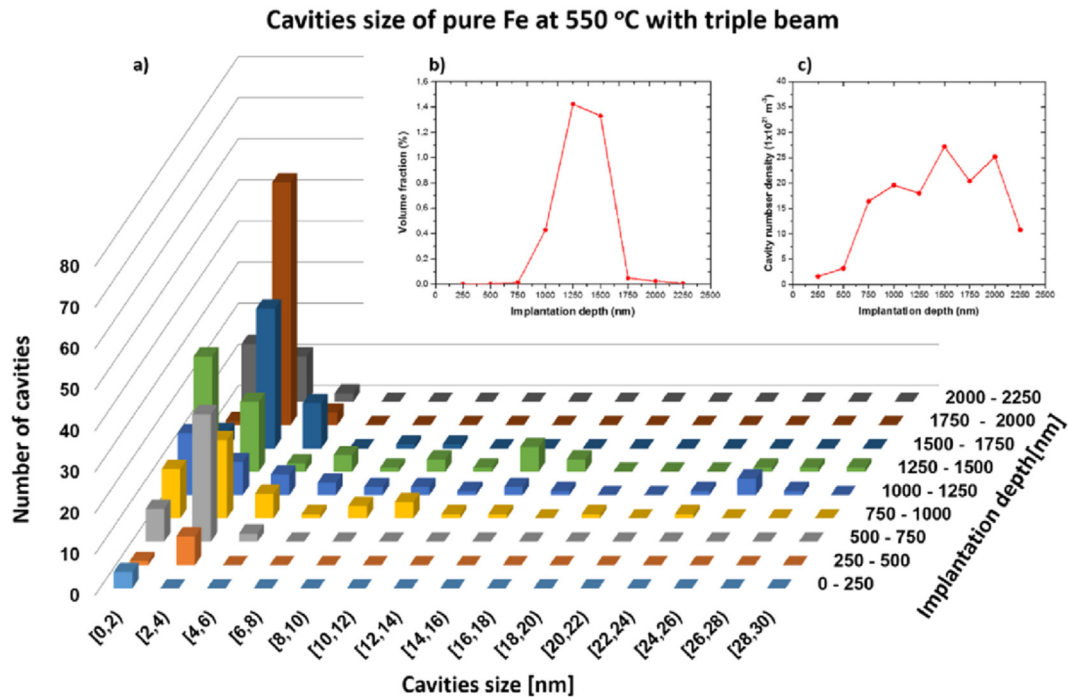


**Fig. 11.** a) Cavity size and b) Volume fraction in function of irradiation depth and c) cavity density number of pure EFDA Fe irradiated by triple ion beams to 40 dpa,  $\sim 14$  He/dpa and  $\sim 50$  H/dpa at 550 °C.

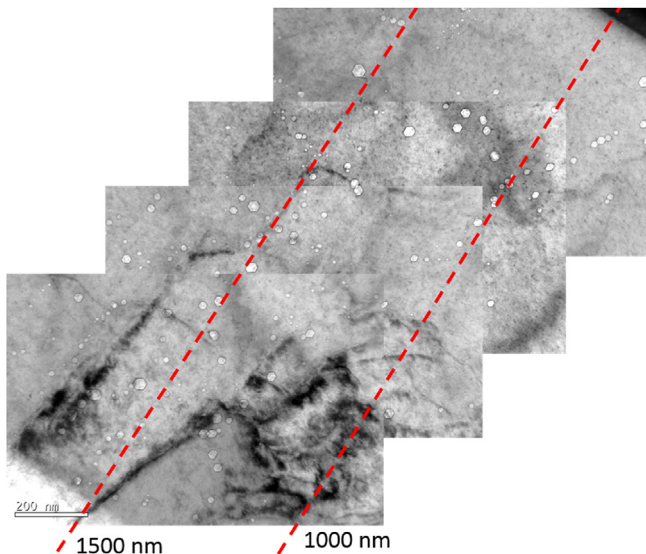


**Fig. 12.** Detail of the cavities distribution on pure EFDA Fe irradiated by triple ion beams to 40 dpa,  $\sim 14$  He/dpa and  $\sim 50$  H/dpa at 550 °C taken from 1 to 1.5  $\mu\text{m}$  depth.

growth [27–29]. Taking into account only Fe implantation, the material showed an area rich in vacancies up to the first micrometer in depth and an area richer in interstitials, due to the injected Fe ions, deeper than 1  $\mu\text{m}$ , as seen in Fig. 13. The contribution of He and H on cavities life-cycle (nucleation, growth and distribution) complicates the picture, since binding and diffusion energies play an important role, particularly after 1  $\mu\text{m}$  in depth, when both He and H were introduced.

Fig. 14 shows the comparison in volume fraction (a) and in cavity number density (b) for all the irradiation temperatures. In each figure, the irradiation profile was included, except for the injected

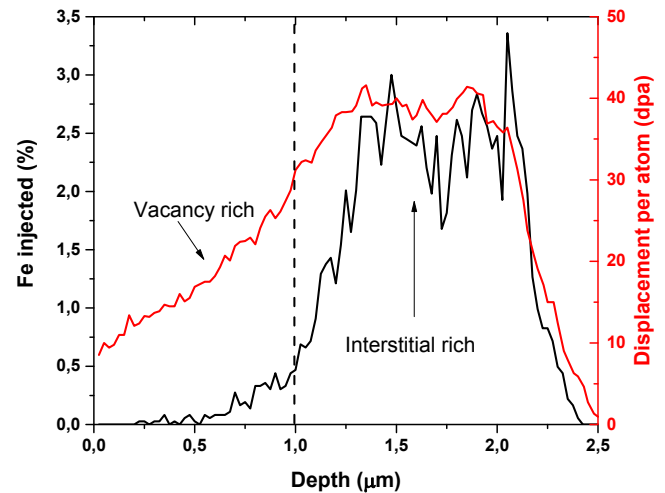


**Fig. 13.** Depth distribution of vacancies in terms of dpa and interstitial generated by Fe ion beam.

interstitials profile seen in Fig. 13, in order to get a better visualization. In those figures it is possible to see that at a temperature of 350 °C, the 0.2% swelling peak is located at a depth of about 500 nm. Deeper than 500 nm, there is a suppression of nucleation of larger cavities, being more extensive, only the nucleation of the smaller ones. At 1500 nm the specimen showed other increase in swelling ( $\sim 0.03\%$ ) but this value is much smaller than the peak mentioned before.

As the irradiation temperature increases, the swelling peak moves deeper into the material, thus increasing its value. At 450 °C, a large value of swelling was measured at 750 nm, possibly due to some large cavities (between 8 and 18 nm) detected in the matrix. This result is possible to explain due to the high amount of

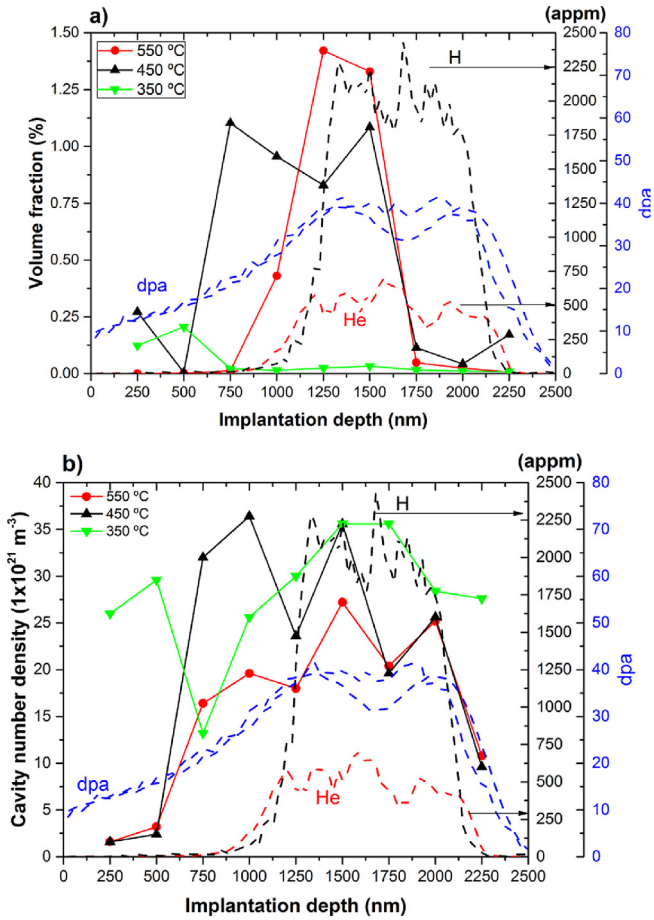


Fig. 14. a) Volume fraction and b) cavity number density on Fe irradiated at 350, 450 and 550 °C with He<sup>+</sup> + H<sup>+</sup> + Fe<sup>3+</sup>.

vacancies created by the Fe beam without He and H, whose diffusion is enhanced by temperature. In fact, at this point the swelling value of 1.1% is the largest measured. Another swelling peak is detected deeper in the material but it is slightly lower (1.08%). Such a high value was not expected; rather one would expect a smaller value which followed the ascending trend in a similar way as the 550 °C swelling profile.

The specimen irradiated at 550 °C showed the maximum swelling value at 1250 nm, which was 1.42%. Then, like the other experiments, the nucleation of large cavities as well as the population were reduced. In any case, the value of swelling measured in this research is distant from the common value of swelling for ferritic-martensitic materials, which is ~0.1%/dpa [30].

If the irradiation profile is taken into account up to 1 μm (where the gases injection is almost negligible), there is a swelling peak due to the nucleation and growth of voids, whose maximum is at 450 °C. Moreover, focusing on the swelling peak at 250 and 2250 nm, again with no influence of gases, there are another two swelling peaks at 450 °C. Clearly the values are much lower, only 0.27 and 0.17% respectively but the dpa values at those depths are lower than 20 dpa.

On the other hand, analyzing the profile between 1 and 2 μm, the maximum peak is produced at 550 °C. Each of the three different temperatures showed a peak. Due to the evolution of the microstructure, it is believed that the cavities detected are HeV clusters; even when the injected interstitials, showed in Fig. 13, were placed and the recombination between those interstitials and

the vacancies is maximum.

Regarding the cavity density number, all the irradiations showed an increase in population, but depending on the temperature, the growth is more extensive or not.

Tanaka et al. [11] measured a maximum swelling of almost 4%, produced during the irradiation at 510 °C on a Fe12%Cr model alloy. Comparing to pure EFDA Fe, a large increase is found, even when Tanaka irradiated a Fe12%Cr alloy which, in theory, is more resistant to irradiation swelling. This phenomenon could be explained by taking into account Tanaka's irradiation profile. In their experiment, light ions (He + H) were introduced before injected self-ions. This produced an increase of recombination of vacancy-interstitial that reduced the swelling value. That result fits with the observations extracted from this research, only if the irradiation profile is studied up to 1 μm.

Regarding preferential nucleation, two clear features were observed. First of all, there are differences on the nucleation of cavities close to the irradiation surface, depending on the irradiation temperature. After an exhaustive microstructural analysis of the outer surface (first 250 nm) of the irradiation depth of each specimen, it was observed that there is a clear variation in both nucleation and size depending on the temperature, which was the only difference between the 3 specimens, besides the change in irradiation setup; as the dpa, He and H levels were maintained at the same depth.

At 350 °C the observations revealed that many cavities

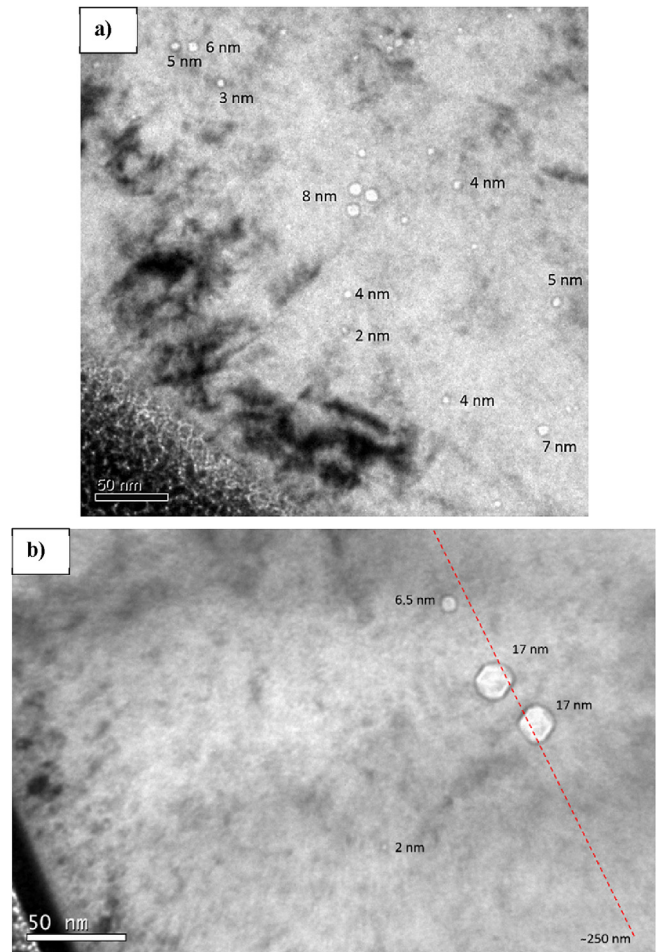


Fig. 15. TEM micrograph of pure EFDA Fe irradiated at a) 350 °C and d) 450 °C showing cavities nucleated very close to the surface.

nucleated very close to the surface (Fig. 15 a). In fact, at this depth this specimen had the highest cavity density number ( $2.6 \times 10^{22} \text{ m}^{-3}$ ). In contrast, specimens irradiated at 450 °C and at 550 °C, despite having the same cavity density number ( $1.6 \times 10^{22} \text{ m}^{-3}$ ) showed a clear difference in the size of the cavities, for instance at 450 °C were found cavities with a very large diameter, 17 nm, as seen in Fig. 15 b). This phenomenon could be attributed to an unexpected local high dislocation density close to the surface or simply to a heterogeneous nucleation due to the irradiation characteristics. For these irradiation conditions, the surface effect acting as vacancy source [31–33] did not give a possible explanation, since the ions used are very energetic and the penetration reaches more than 2  $\mu\text{m}$ , deep enough to neglect any influence of the surface.

Furthermore, it has been proved that irradiation using a defocused beam, rather than using raster beams with a certain sweep frequency, produces a microstructural evolution more similar to that produced by neutron irradiation [34,35]. The irradiation at JANNuS facility was performed using three defocused beams, in order to have comparable results between neutron and ion irradiation, taking into account that the cases are not exactly the same. For this type of set-up, it is very important to avoid undesirable effects as much as possible. However, due to the high complexity of the experiment, it is possible to produce a nonhomogeneous nucleation.

The second observed feature was the nucleation on microstructural characteristics such as dislocations and grain boundaries. The effect of dislocations on cavity nucleation has been observed experimentally under triple beam irradiation, with a cold rolled specimen that showed more resistance to irradiation swelling than other specimens in as-received condition [36]. That effect is explained easily by the enhancement of trapping point defects.

The results of this research revealed that the irradiation at 350 °C does not produce a clear alignment of cavities. However, an arrangement of nucleation clusters was observed at 1.5  $\mu\text{m}$  (Fig. 5) but it was not close to the surface (Fig. 4) where the cavities nucleated randomly. Therefore, the nucleation and growth mechanism seems to be different depending on the irradiation damage and temperature. On the other hand, at 450 °C the nucleation in clusters is more significant, as seen in Fig. 7. Finally, at 550 °C, the cavities showed a clear alignment, probably along defect sinks such as dislocations, as shown in Fig. 16 within the red rectangle. However, specifying which defect sink was acting is almost

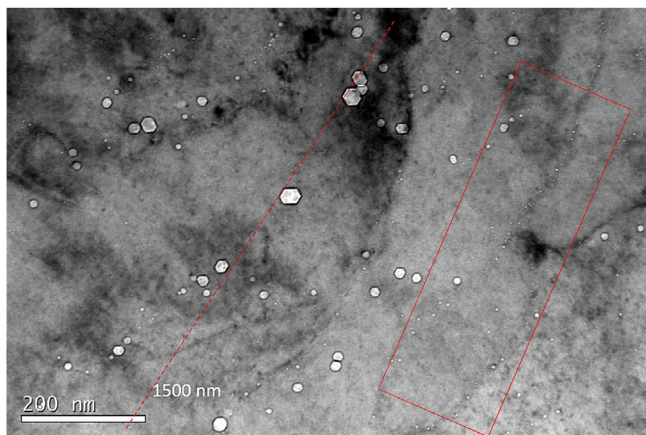


**Fig. 16.** TEM micrograph taken from the specimen irradiated at 550 °C showing sub-grain structure whose boundaries are decorated with very small cavities, highlighted by a red rectangle. (For interpretation of the references to colour in this figure legend, the reader is referred to the web version of this article.)

impossible. On the other hand, the use of degraders may interfere in the homogeneity of the irradiation, but this effect, as well as the aforementioned, is hard to quantify. The largest cavities also were aligned but due to their size, it is more difficult to notice, as seen in Fig. 17.

Other interesting feature is the fact that there is a clear depletion of small cavities nearby the large ones at 450 and 550 °C, which seems to indicate a resolution of the small ones if they are close or around larger ones. As an example of this effect, in Fig. 18 (highlighted with red arrows) and Fig. 19 it is possible to observe large and medium size cavities with very small ones around of them at 450 °C and 550 °C respectively. This phenomenon is called Ostwald ripening [37] and it is observed when large bubbles increase their diameter while the smaller ones shrink or even disappear.

Regarding the cavity shape, since their growth is affected by the irradiation temperature, it was also found that the cavities will present circular or polygonal faceted shape, depending on the temperature. At 350 °C all of the observed ones were circular with a maximum size of 18 nm. At 450 °C, cavities of different shapes coexisted, the largest circular cavity had a diameter of 21 nm, and the smallest faceted cavity had a diameter of 17 nm. Finally, at 550 °C, the largest cavity was faceted-shaped with a diameter of 30 nm (Fig. 19), the smallest faceted cavity had a diameter of 15 nm and the smallest round-shaped cavity had a diameter of 17 nm. These observations lead to think that the diameter limit at which the cavities shift their shape from circular to polygonal goes from 16 nm up to 18 nm. It is believed that the evolution of the cavity shape is related to the thermodynamic equilibrium between the superficial pressure of the cavity and the matrix. Besides, it is well-known that the internal pressure of a cavity depends completely of the ratio He/V. Therefore, the following step of this work is to try to measure the amount of He/H ratio and the cavity pressure to distinguish between void and bubble using techniques such as EELS [38,39]. In contrast to He that can be analyzed on HRTEM by EELS [39], H studies require other techniques such as Positron Annihilation Spectroscopy (PAS) [40] or by means of a nuclear resonance reaction after the irradiation [36], always taking into account that probably most of the H is released from the specimen due to its

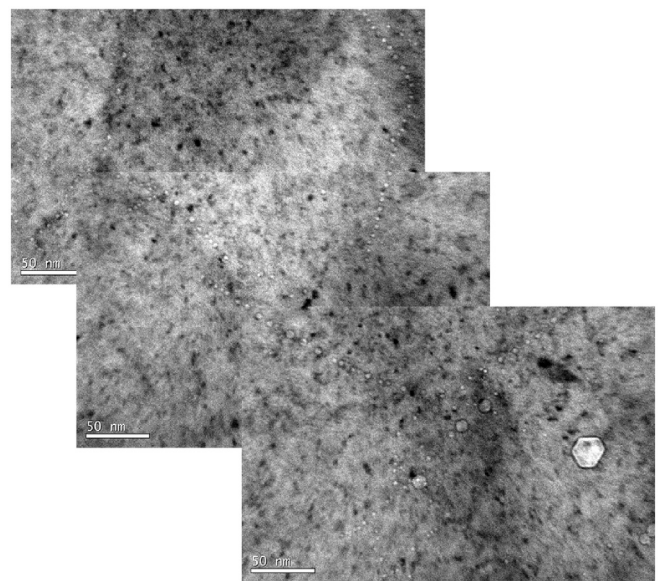


**Fig. 17.** TEM micrographs of the specimen irradiated at 550 °C showing very clear alignment of cavities along with medium and large cavities grouped in clusters at 2  $\mu\text{m}$  depth.

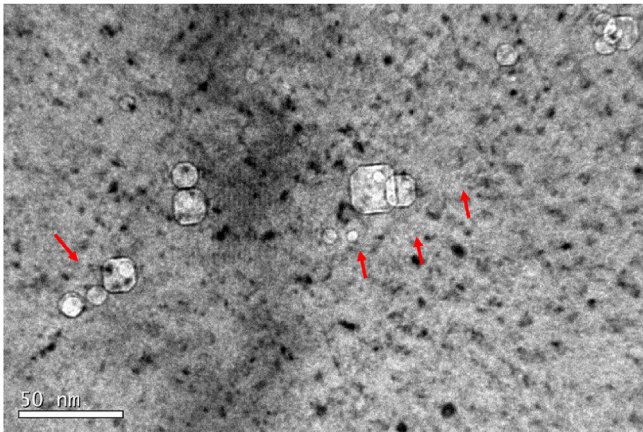


**Fig. 18.** TEM micrograph of pure EFDA Fe irradiated with triple beam at 450 °C showing a resolution and growth of cavities.

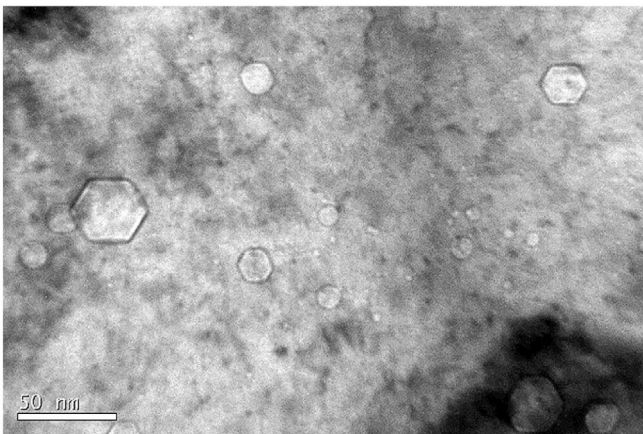


**Fig. 19.** TEM micrograph on bright field underfocused of pure EFDA Fe irradiated at 550 °C, showing different cavities shape.

high diffusivity, especially at high temperatures.

As a matter of fact, Fréchet et al. [38] found a linear relationship between pressure and density of He atoms on bubbles, which decreases significantly up to bubbles with a radius of 5 nm in an He implanted steel. Extrapolating those results along with the observations carried out here, the ratio between He and vacancies can be lower than 1 for the largest cavities detected in this work, indicating possibly bubble-void conversion.

Due to the difficulty of the experimental observation of diffusion, nucleation and growth of defects produced by helium and hydrogen, together with vacancies and their interaction with microstructural sinks as dislocations or grain boundaries, it is necessary to have modeling studies to find a possible explanation of the microstructural observations. In fact, the experiment carried out in this research was aimed to be experimental back up for modeling studies, since the material used, pure Fe, is one of the most common materials used for modeling because it is the base of the RAFM structural material for the future nuclear fusion reactors.

Taking into account modeling results on H [41–43] and He [44–46] in the form of clusters attached to vacancies ( $\text{He}_n\text{V}_m$  and  $\text{H}_j\text{V}_m$  respectively), it has been reported that both of them tend to stabilize the aforementioned clusters found in the matrix. In fact, it seems that as the amount of gas increases, the binding energy between gas and vacancy also increases. On the other hand, the Fe

atoms, which belong to the matrix, arranged around the same clusters, are less bound to their lattice sites, increasing the chances to be emitted into the material as self-interstitial; in other words, the loop punching phenomena is increased.

However, the effect of He and H injected together in the materials makes the overall picture more difficult to understand. Again, using modeling results, it is observed that there is an interaction between both gases and hence, their binding energy to vacancies, interstitials and each other, depends strongly on the amount of gas atoms [47]. On the other hand, in the mentioned research, a remarkable result was obtained with respect to the distribution of He and H inside a Fe matrix. They have observed a core of He atoms surrounded by a shell of H, attracted by the free surface of the bubble. However, the experimental agreement is nowadays almost impossible to achieve. If the creation of vacancies (dpa) and the injection of interstitials is added to those interactions at the same time (by means of self-ion irradiation) the interpretation of the results is still harder.

Regarding experimental results with triple beams, it has been observed by Tanaka et al. [11] a synergetic effect when introducing simultaneously He, H and Fe ions on Fe9Cr and Fe19Cr alloys. This is explained by an increase in defect collecting efficiency or in dislocation bias. The microstructural results are clearly different from the observations in which double irradiation was performed (Fe + He and Fe + H). In fact, the simultaneous irradiation with Fe and H, did not modify the microstructure. No cavities nor dislocations were observed, which means that regarding swelling, there is no effect. The swelling peak was observed at 510 °C, which is in good agreement with the swelling results obtained in this research. Additionally, the large cavity detected came from the specimen irradiated at 550 °C, whose diameter was around 28 nm. The aforementioned synergistic effect between He and H has been observed by E. Wakai [35] in ferritic materials and in vanadium [48] as well.

Y.E. Kupriyanova et al. [49] studied the effect of both double and triple beam irradiation on more complex steels, such as the ferritic-martensitic alloys F82H, Rusfer EK181 and EP45. Afterwards, they have observed that both He and H increased the void swelling when the ion gases were introduced separately. However, when both ions were implanted simultaneously, the effect observed on swelling was lower, suggesting a complementary effect that depends on the injected amount of H. If this amount is very high (~1%) then a suppression in swelling is measured.

Focusing on the microstructural observations, it seems that the addition of hydrogen plus helium reduces the critical cavity size or changes the diffusion bias for vacancy accumulation at bubble embryos [50]. Hydrogen, hence, tends to enhance the production of smaller cavities compared to He. This effect is probably due to the greater mobility of H. So, when He and H were injected together, the size and population density seem to be biased by He while H was retained in nucleated voids. On the other hand, there is a critical parameter to take into account when comparing all of the aforementioned results with the ones presented here, and it is the effect of alloying elements that may act as irradiation defect suppressors. Especially in the case of the ferritic martensitic, where in addition, the material has a complex microstructure in contrast with the ferritic microstructure with very large grains and low dislocation density of the pure EFDA Fe.

Although the effect of implanted H on microstructure is very hard to detect, its effect on mechanical properties has been proved. For example, it reduces the elongation to fracture and produces different phenomena in terms of fracture surface depending on the material [51,52].

## 5. Conclusions

The most important conclusions arising from this research are:

- A novel methodology is presented in this paper in order to improve the quantification of swelling on irradiated materials due to the nucleation of cavities, as shown in other experiments with dual or triple beams setup [53–55]. Since the lamella path was divided into bins (of 250 nm) it is possible to correlate the simulation results in terms of simulated dpa, He and H levels with the microstructural observations.
- Cavity formation at 350 °C does not match with the expected simulation completely. The largest defects were found in the first 750 nm. A random distribution of small cavities (2–4 nm) within the matrix was observed beyond 750 nm.
- Irradiation at 450 and 550 °C leads to preferential nucleation, and especially at 550 °C cavity nucleation around grain boundaries is much more extensive.
- There is a clear temperature effect on cavity growth. As the irradiation temperature increases, the average size of the cavities detected also increases and hence, the volume fraction increases in the implanted region. The maximum peak swelling is produced at 550 °C with a value of 1.4%.
- The cavities change their morphology at 450 and 550 °C from circular to faceted at a diameter between 16 and 18 nm.
- There are some questions that remain about the effect of hydrogen on the stabilization of cavity growth. It turns out that it is necessary to repeat the irradiations but only using He and Fe ion beams and carrying out an exhaustive comparison between the microstructural observations presented in this paper and the further new ones.

## Acknowledgements

This work was carried out within the framework of the EURO-fusion Consortium and has received funding from the Euratom Research and Training Programme 2014–2018 under grant agreement number 633053. The views and opinions expressed herein do not necessarily reflect those of the European Commission.

## References

- [1] R.J.M. Konings, et al., *Comprehensive Nuclear Materials*, vol. 5, Elsevier, Amsterdam, 2012.
- [2] M.J. Fluss, L.L. Hsiung, J. Marian, *Dual and Triple Ion-beam Irradiations of Fe, Fe(Cr) and Fe(Cr)-ODS Final Report: IAEA SMORE CRP*, 2011.
- [3] I.S. Kim, et al., Defect and void evolution in oxide dispersion strengthened ferritic steels under 3.2 MeV Fe<sup>+</sup> ion irradiation with simultaneous helium injection, *J. Nucl. Mater.* 280 (3) (2000) 264–274.
- [4] R.L. Simons, H.R. Brager, W.Y. Matsumoto, Design of a single variable helium effects experiment for irradiation in FFIF using alloys enriched in nickel-59, *J. Nucl. Mater.* 141–143 (Part 2) (1986) 1057–1060.
- [5] E. Wakai, et al., Radiation hardening and embrittlement due to He production in F82H steel irradiated at 250 °C in JMTR, *J. Nucl. Mater.* 343 (1–3) (2005) 285–296.
- [6] N. Hashimoto, R.L. Klueh, K. Shiba, Pro and cons of Ni and B doping to study helium effects in ferritic martensitic steels, *J. Nucl. Mater.* 307–311 (2002) 7.
- [7] R.J. Kurtz, et al., The transport and fate of helium in martensitic steels at fusion relevant He/dpa ratios and dpa rates, *J. Nucl. Mater.* 367–370 (2007) 417–422.
- [8] Y. Dai, G.S. Bauer, Status of the first SINQ irradiation experiment, STIP-I, *J. Nucl. Mater.* 296 (1–3) (2001) 43–53.
- [9] Y. Dai, et al., The second SINQ target irradiation program, STIP-II, *J. Nucl. Mater.* 343 (1–3) (2005) 33–44.
- [10] V. Krsjak, et al., Helium behavior in ferritic/martensitic steels irradiated in spallation target, *J. Nucl. Mater.* 456 (0) (2015) 382–388.
- [11] T. Tanaka, et al., Synergistic effect of helium and hydrogen for defect evolution under multi-ion irradiation of Fe–Cr ferritic alloys, *J. Nucl. Mater.* 329–333 (Part A(0)) (2004) 294–298.
- [12] F.A. Garner, J.J. Laidler, Review of neutron and charged particle intercorrelation programs. Proceedings of the Workshop on Correlation of Neutron and Charged Particle Damage, Oak Ridge National Laboratory, 1976.
- [13] M.B. Lewis, A method for simulating fusion reactor radiation damage using triple ion beams, *IEEE Trans. Nucl. Sci.* 26 (1) (1979) 1320–1322.
- [14] K. Farrell, M.B. Lewis, The hydrogen content of austenite after cathodic charging, *Scr. Metall.* 15 (6) (1981) 661–664.
- [15] L.L. Horton, J. Bentley, W.A. Jesser, The microstructure of “triple-beam” ion irradiated Fe and Fe–Cr alloys, *J. Nucl. Mater.* 104 (0) (1981) 1085–1089.
- [16] L.L. Horton, J. Bentley, W.A. Jesser, The depth distribution of displacement damage in  $\alpha$ -iron under “triple beam” ion irradiation, *J. Nucl. Mater.* 104 (C) (1981) 1343–1347.
- [17] L.L. Horton, J. Bentley, K. Farrell, A TEM study of neutron-irradiated iron, *J. Nucl. Mater.* 108–109(C) (1982) 222–233.
- [18] M.B. Lewis, et al., Triple ion beam irradiation facility, *Nucl. Inst. Methods Phys. Res. B* 43 (2) (1989) 243–253.
- [19] S. Hamada, et al., Development of a triple beam irradiation facility, *J. Nucl. Mater.* 258–263 (PART 1 A) (1998) 383–387.
- [20] N. Sekimura, et al., The effect of helium on the microstructural evolution in PCA as studied by dual beam irradiation, *J. Nucl. Mater.* 122 (1–3) (1984) 322–326.
- [21] Y. Katoh, et al., The influence of He co-implantation on ion-induced hardening of low activation ferritic steel evaluated by micro-indentation technique, *J. Nucl. Mater.* 271 (1999) 5.
- [22] M. Ando, et al., Evaluation of hardening behaviour of ion irradiated reduced activation ferritic/martensitic steels by an ultramicroindentation technique, *J. Nucl. Mater.* 307–311 (2002) 6.
- [23] J.P. Hirth, Effects of hydrogen on the properties of iron and steel, *Metall. Trans. A* 11 (6) (1980) 861–890.
- [24] J. Le Coze, Procurement of Pure Fe Metal and Fe-based Alloys with Controlled Chemical Alloying Element Contents and Microstructure, in Final Report on Model Alloy Preparation, 2007.
- [25] L. Beck, et al., Ion irradiation and radiation effect characterization at the JANNUS-Saclay triple beam facility, *J. Mater. Res.* 30 (09) (2015) 1183–1194.
- [26] C.H.M. Broeders, A.Y. Konobeyev, Defect production efficiency in metals under neutron irradiation, *J. Nucl. Mater.* 328 (2–3) (2004) 197–214.
- [27] L. Shao, et al., Effect of defect imbalance on void swelling distributions produced in pure iron irradiated with 3.5 MeV self-ions, *J. Nucl. Mater.* 453 (1–3) (2014) 176–181.
- [28] F.A. Garner, Impact of the injected interstitial on the correlation of charged particle and neutron-induced radiation damage, *J. Nucl. Mater.* 117 (1983) 177–197.
- [29] A.D. Brailsford, L.K. Mansur, Effect of self-ion injection in simulation studies of void swelling, *J. Nucl. Mater.* 71 (1) (1977) 110–116.
- [30] R.L. Klueh, D.R. Harries, High-chromium Ferritic and Martensitic Steels for Nuclear Applications. Monograph, ASTM, W. Conshohocken, PA, 2001, 221 pp.
- [31] R.E. Stoller, The effect of free surfaces on cascade damage production in iron, *J. Nucl. Mater.* 307–311 (Part 2) (2002) 935–940.
- [32] M.J. Aliaga, M.J. Caturla, R. Schäublin, Surface damage in TEM thick  $\alpha$ -Fe samples by implantation with 150 keV Fe ions, *Nucl. Instrum. Methods Phys. Res. Sect. B Beam Interact. Mater. Atoms* 352 (2015) 217–220.
- [33] M.J. Aliaga, et al., Surface-induced vacancy loops and damage dispersion in irradiated Fe thin films, *Acta Mater.* 101 (2015) 22–30.
- [34] E. Getto, et al., Effect of irradiation mode on the microstructure of self-ion irradiated ferritic-martensitic alloys, *J. Nucl. Mater.* 465 (2015) 116–126.
- [35] J.G. Gigax, et al., The influence of ion beam rastering on the swelling of self-ion irradiated pure iron at 450 °C, *J. Nucl. Mater.* 465 (2015) 343–348.
- [36] E. Wakai, et al., Swelling behavior of F82H steel irradiated by triple/dual ion beams, *J. Nucl. Mater.* 318 (0) (2003) 267–273.
- [37] H. Trinkaus, B.N. Singh, Helium accumulation in metals during irradiation – where do we stand? *J. Nucl. Mater.* 323 (2–3) (2003) 229–242.
- [38] S. Fréchet, et al., Study by EELS of helium bubbles in a martensitic steel, *J. Nucl. Mater.* 393 (1) (2009) 102–107.
- [39] W. Jäger, et al., Density and pressure of helium in small bubbles in metals, *J. Nucl. Mater.* 111–112 (0) (1982) 674–680.
- [40] V. Slugeň, S. Pecko, S. Sojak, Experimental studies of irradiated and hydrogen implantation damaged reactor steels, *J. Nucl. Mater.* 468 (2016) 285–288.
- [41] E. Hayward, C.S. Deo, The Energetics of Hydrogen–vacancy Clusters in BCC Iron, MRS Online Proceedings Library, 2011, 1363: p. null-null.
- [42] B. Irigoyen, et al., The interaction of hydrogen with an Fe vacancy: a molecular orbital simulation, *J. Phys. D Appl. Phys.* 29 (5) (1996) 1306.
- [43] E. Hayward, C.-C. Fu, Interplay between hydrogen and vacancies in alpha-Fe, *Phys. Rev. B* 87 (17) (2013) 174103.
- [44] G. Lucas, R. Schäublin, Stability of helium bubbles in alpha-iron: a molecular dynamics study, *J. Nucl. Mater.* 386–388 (0) (2009) 360–362.
- [45] K. Morishita, R. Sugano, B.D. Wirth, MD and KMC modeling of the growth and shrinkage mechanisms of helium–vacancy clusters in Fe, *J. Nucl. Mater.* 323 (2–3) (2003) 243–250.
- [46] K. Morishita, et al., Thermal stability of helium–vacancy clusters in iron, *Nucl. Instrum. Methods Phys. Res. Sect. B Beam Interact. Mater. Atoms* 202 (0) (2003) 76–81.
- [47] H. Erin, D. Chaitanya, Synergistic effects in hydrogen–helium bubbles, *J. Phys. Condens. Matter* 24 (26) (2012) 265402.
- [48] N. Sekimura, et al., Synergistic effects of hydrogen and helium on microstructural evolution in vanadium alloys by triple ion beam irradiation, *J. Nucl. Mater.* 283–287 (Part 1(0)) (2000) 224–228.
- [49] Y.E. Kupriyanova, et al., Use of double and triple-ion irradiation to study the influence of high levels of helium and hydrogen on void swelling of 8–12% Cr

- ferritic-martensitic steels, *J. Nucl. Mater.* 468 (2016) 264–273.
- [50] J. Marian, et al., A review of helium–hydrogen synergistic effects in radiation damage observed in fusion energy steels and an interaction model to guide future understanding, *J. Nucl. Mater.* 462 (0) (2015) 409–421.
- [51] [E. Malitckii, Y. Yagodzinsky, H. Hänninen, Hydrogen-induced crack nucleation in tensile testing of EUROFER 97 and ODS-EUROFER steels at elevated temperature, \*J. Nucl. Mater.\* 466 \(2015\) 286–291.](#)
- [52] Y. Yagodzinsky, et al., Hydrogen effects on tensile properties of EUROFER 97 and ODS-EUROFER steels, *J. Nucl. Mater.* 444 (1–3) (2014) 435–440.
- [53] D. Brimbal, et al., He and Cr effects on radiation damage formation in ion-irradiated pure iron and Fe–5.40 wt.% Cr: a transmission electron microscopy study, *Acta Mater.* 61 (13) (2013) 4757–4764.
- [54] E. Wakai, et al., Effect of triple ion beams in ferritic-martensitic steel on swelling behavior, *J. Nucl. Mater.* 307–311 (2002) 5.
- [55] [M. Ando, et al., Synergistic effect of displacement damage and helium atoms on radiation hardening in F82H at TIARA facility, \*J. Nucl. Mater.\* 329–333 \(2004\) 1137–1141.](#)